Spin-driven nematic instability of the multiorbital Hubbard model: Application to iron-based superconductors

Morten H. Christensen, Jian Kang, Brian M. Andersen, and Rafael M. Fernandes

Phys. Rev. B **93**, 085136 — Published 25 February 2016

DOI: 10.1103/PhysRevB.93.085136

Spin-Driven Nematic Instability of the Multi-Orbital Hubbard Model: Application to Iron-Based Superconductors

Morten H. Christensen,[1,2] Jian Kang,[1] Brian M. Andersen,[2] and Rafael M. Fernandes[1]

[1] *School of Physics and Astronomy, University of Minnesota, Minneapolis, MN 55455, USA*
[2] *Niels Bohr Institute, University of Copenhagen, Juliane Maries Vej 30, DK-2100, Denmark*

Nematic order resulting from the partial melting of density-waves has been proposed as the mechanism to explain nematicity in iron-based superconductors. An outstanding question, however, is whether the microscopic electronic model for these systems – the multi-orbital Hubbard model – displays such an ordered state as its leading instability. In contrast to usual electronic instabilities, such as magnetic and charge order, this fluctuation-driven phenomenon cannot be captured by the standard RPA method. Here, by including fluctuations beyond RPA in the multi-orbital Hubbard model, we derive its nematic susceptibility and contrast it with its ferro-orbital order susceptibility, showing that its leading instability is the spin-driven nematic phase. Our results also demonstrate the primary role played by the d_{xy} orbital in driving the nematic transition, and reveal that high-energy magnetic fluctuations are essential to stabilize nematic order in the absence of magnetic order.

The elucidation of electronic Ising-nematic order [1] – the state in which electronic degrees of freedom spontaneously lower the point-group symmetry of the system – has become an important problem in unconventional superconductors [2, 3]. In both pnictides [4–9] and cuprates [10–12], the experimentally observed nematic order has been proposed to arise from the partial melting of an underlying spin density-wave (SDW) [13–16] or charge density-wave (CDW) [17–19] stripe-order. This mechanism is based on robust symmetry considerations. Consider for concreteness the stripe SDW case: the ground state has an $O(3) \times Z_2$ degeneracy, with $O(3)$ denoting the direction of the magnetic order parameter in spin space, and Z_2 denoting the selection of the SDW ordering vector $\mathbf{Q}_X = (\pi, 0)$ or $\mathbf{Q}_Y = (0, \pi)$ (in the CDW case, the system has an $O(2) \times Z_2$ degeneracy). Fluctuations in layered systems suppress the continuous ($O(3)$ or $O(2)$) and the discrete (Z_2) symmetries differently, favoring an intermediate regime in which only the Z_2 symmetry is broken [13]. Because the Z_2 symmetry distinguishes between two ordering vectors related by a 90° rotation, its breaking implies a tetragonal-to-orthorhombic transition, and therefore nematic order.

Although this mechanism for spin-driven (or charge-driven) nematic order has been established in simplified low-energy models for pnictides [13–15, 20, 21] and cuprates [18, 19], it remains hotly debated whether more realistic microscopic models display nematic order as the leading electronic instability. the cuprates, a sensible microscopic model is the single-band Hubbard model, whose phase diagram has been reported to display nematic correlations in the strong-coupling regime [22, 23]. For the pnictides, due to the $3d^6$ configuration of Fe and to the small crystal field splittings, a five-orbital Hubbard model, including Hund's rule interactions, is a more appropriate starting point [24, 25]. Furthermore, because many pnictides display metallic behavior, a weak-coupling analysis of this intricate model can reveal important information about the underlying physics of these materials. Indeed, conventional RPA approaches have been employed to study the onset of SDW, CDW, and ferromagnetism. However, in contrast to these usual electronic instabilities, the standard RPA approach does not capture the nematic instability even qualitatively, as we show below, making it difficult to assess whether the realistic multi-orbital Hubbard model has a tendency towards nematic order.

In this Letter, we extend the standard RPA approach and derive the nematic susceptibility of an arbitrary multi-orbital Hubbard model. The fluctuations included in this formalism arise solely from the non-interacting part of the Hamiltonian, such that interactions are treated at the same order as in the typical RPA method. We apply this formalism to the case of SDW-driven nematicity in iron pnictides, and establish that the leading instability of the five-orbital interacting model is a spin-driven nematic phase for a wide range of parameters. In general, we find that nematic order exists in a narrow T range above the magnetic transition line, in agreement with experiments in the pnictides [26]. However, magnetic fluctuations at higher energies can induce a sizable splitting between the two transitions, particularly in the regime where the SDW transition is suppressed to zero. We propose that this effect may be relevant to understanding the unusual nematic phase of FeSe [27–31]. Previously, the investigation of the multi-orbital Hubbard model in Ref. [21] revealed the importance of the orbital content of the Fermi surface in the low-energy spin-nematic model of the pnictides. Here, we find from the orbitally-resolved nematic susceptibility that whereas the d_{xz}, d_{yz}, and d_{xy} orbitals contribute almost equally to the SDW instability, the d_{xy} orbital plays a stronger role in driving the nematic instability. Finally, we compare the nematic susceptibility with the RPA-derived ferro-orbital order susceptibility. work provides a promising route to search for nematicity in different compounds, as it is compatible with *ab initio* approaches and also with methods that include the effects of moderate interactions, such as LDA+DMFT [32, 33].

Our starting point is the multi-orbital Hubbard model

with onsite interactions [25, 34]. The non-interacting part is given by $\mathcal{H}_0 = \sum_{\mu,\nu}(\epsilon_{\mu\nu}(\mathbf{k}) - \tilde{\epsilon}\delta_{\mu\nu})\, c^\dagger_{\mathbf{k}\mu\sigma} c_{\mathbf{k}\nu\sigma}$, where $c^\dagger_{\mathbf{k}\mu\sigma}$ creates an electron with momentum $\mathbf{k}$ and spin σ at orbital $\mu = 1, ..., N_{\rm orb}$ and the hopping parameters $\epsilon_{\mu\nu}(\mathbf{k})$ are determined from tight-binding fits to *ab initio* calculations (sums over spin and momentum indices are left implicit). The four onsite interaction terms correspond to the intra-orbital Hubbard term, $\mathcal{H}_U = U\sum_\mu n_{\mathbf{q}\mu\uparrow} n_{-\mathbf{q}\mu\downarrow}$, the inter-orbital Hubbard term, $\mathcal{H}_{U'} = U'\sum_{\mu<\nu} n_{\mathbf{q}\mu\sigma} n_{-\mathbf{q}\nu\sigma'}$, the Hund's rule coupling, $\mathcal{H}_J = J\sum_{\mu<\nu} c^\dagger_{\mathbf{k}+\mathbf{q}\mu\sigma} c_{\mathbf{k}\nu\sigma} c^\dagger_{\mathbf{k}'-\mathbf{q}\nu\sigma'} c_{\mathbf{k}'\mu\sigma'}$, and the pair-hopping term $\mathcal{H}_{J'} = J'\sum_{\mu<\nu} c^\dagger_{\mathbf{k}+\mathbf{q}\mu\sigma} c^\dagger_{\mathbf{k}'-\mathbf{q}\mu\bar{\sigma}} c_{\mathbf{k}'\nu\bar{\sigma}} c_{\mathbf{k}\nu\sigma}$. These coefficients are related by $U' = U - 2J$ and $J' = J$. Previous approaches considered the nematic susceptibility of a spin-fermion model [35]; here, we will focus on the Hubbard model within RPA. The mechanism in which nematic order arises from the partial melting of an SDW or a CDW requires fluctuations at two momenta related by 90°, in general $\mathbf{Q}_1 = \left(\frac{\pi}{n}, 0\right)$ and $\mathbf{Q}_2 = \left(0, \frac{\pi}{n}\right)$, with integer n. Although our formalism can be extended in a straightforward way to arbitrary n, hereafter we focus on $n = 1$. to make contact with the pnictides, we consider the SDW channel. Performing a Hartree-Fock decoupling of $\mathcal{H}$ in both the $\mathbf{q} = 0$ charge channel and the $\mathbf{q} = \mathbf{Q}_i$ SDW channel:

$$\begin{aligned}\mathcal{H}^{\rm MF} = &\sum_{\mathbf{k}} (\epsilon_{\mu\nu}(\mathbf{k}) - \tilde{\epsilon}_\nu \delta_{\mu\nu})\, c^\dagger_{\mathbf{k}\mu\sigma} c_{\mathbf{k}\nu\sigma} \\ &- \frac{1}{2}\sum_{\mathbf{kq}} \mathbf{M}^i_{\mathbf{q}\,\mu} \cdot c^\dagger_{\mathbf{k}-\mathbf{q}+\mathbf{Q}_i\mu\sigma} \boldsymbol{\sigma}_{\sigma\sigma'} c_{\mathbf{k}\mu\sigma'}\,, \qquad (1)\end{aligned}$$

where $\tilde{\epsilon}_\nu$ incorporates the changes in the mean-field densities and $\mathbf{M}^i_{\mathbf{q}\,\mu} = \frac{1}{2}\sum_{\mathbf{k}} U^\rho_\mu \langle c^\dagger_{\mathbf{k}+\mathbf{q}+\mathbf{Q}_i\rho\sigma} \boldsymbol{\sigma}_{\sigma\sigma'} c_{\mathbf{k}\rho\sigma'}\rangle$ are the SDW order parameters with $i = X, Y$. The interaction matrix U^ρ_μ is $U^a_a = U$ and $U^a_{b\neq a} = J$. We consider only intra-orbital magnetism, since previous Hartree-Fock calculations revealed that in the ground state the intra-orbital SDW order parameters are the dominant ones [34]. In the standard RPA approach for the SDW instability, the electronic degrees of freedom are integrated out, yielding the quadratic magnetic free energy:

$$F^{(2)}_{\rm mag}[\mathbf{M}^i_\mu] = \sum_{q, i=X,Y} [\chi^{\mu\nu}_i(q)]^{-1}\, \mathbf{M}^i_{q,\mu} \cdot \mathbf{M}^i_{-q,\nu}\,, \qquad (2)$$

with the magnetic propagator $\chi^{\mu\nu}_i(q)$

$$\chi^{\mu\nu}_i(q) = \left[(U^\mu_\nu)^{-1} + \sum_k \mathcal{G}^{\nu\mu}(k)\mathcal{G}^{\mu\nu}_i(k+q)\right]^{-1}, \qquad (3)$$

where $\mathcal{G}^{\mu\nu}_i(k) \equiv \mathcal{G}^{\mu\nu}(k + \mathbf{Q}_i)$ is the Green's function in orbital basis, $q = (\mathbf{q}, \Omega_n)$, $\sum_q = T/N_{\mathbf{q}} \sum_{\mathbf{q}} \sum_{\Omega_n}$, and $\Omega_n = 2n\pi T$ is the Matsubara frequency. The RPA magnetic susceptibility $\langle \mathbf{M}^i_{q,\mu} \cdot \mathbf{M}^i_{-q,\nu}\rangle$ is proportional to and diverges at the same temperature as the magnetic propagator $\chi^{\mu\nu}_i(q)$. Note that the tetragonal symmetry of the system implies that a peak of $\chi^{\mu\nu}_i(q)$ at $\mathbf{Q}_X = (\pi, 0)$ will be accompanied by an equal peak at $\mathbf{Q}_Y = (0, \pi)$. Therefore, at this order in perturbation theory, the system does not distinguish the case in which either $\mathbf{Q}_X$ or $\mathbf{Q}_Y$ is selected (single-$\mathbf{Q}$ order) from the case in which both are selected (double-$\mathbf{Q}$ order), i.e. the standard RPA approach is blind to nematicity. To remedy this problem, we go beyond the second-order expansion of the free energy and calculate the quartic-order terms:

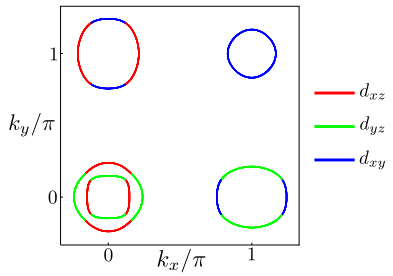

FIG. 1. (Color online) Normal-state Fermi surface based on the parameters of Ikeda *et al.* [44]. The colors indicate the dominant orbital contribution.

$$\begin{aligned}F^{(4)}_{\rm mag}[\mathbf{M}^X_\mu, \mathbf{M}^Y_\mu] = &\frac{1}{2} u^{\rho\nu\eta\mu} \left(\mathbf{M}^X_\rho \cdot \mathbf{M}^X_\nu + \mathbf{M}^Y_\rho \cdot \mathbf{M}^Y_\nu\right) \\ &\times \left(\mathbf{M}^X_\eta \cdot \mathbf{M}^X_\mu + \mathbf{M}^Y_\eta \cdot \mathbf{M}^Y_\mu\right) \\ &- \frac{1}{2} g^{\rho\nu\eta\mu} \left(\mathbf{M}^X_\rho \cdot \mathbf{M}^X_\nu - \mathbf{M}^Y_\rho \cdot \mathbf{M}^Y_\nu\right) \\ &\times \left(\mathbf{M}^X_\eta \cdot \mathbf{M}^X_\mu - \mathbf{M}^Y_\eta \cdot \mathbf{M}^Y_\mu\right) \\ &+ 2 w^{\rho\nu\eta\mu} \left(\mathbf{M}^X_\rho \cdot \mathbf{M}^Y_\nu\right)\left(\mathbf{M}^X_\eta \cdot \mathbf{M}^Y_\mu\right)\,, \qquad (4)\end{aligned}$$

The quartic coefficients, whose expressions are shown explicitly in Appendix A, depend only on the non-interacting Green's functions. Although interactions can also contribute to them, as shown in Refs. [36, 37], within the RPA approach these contributions are subleading and can be neglected. The most relevant coefficient for the nematic instability is $g^{\rho\nu\eta\mu}$, whose term distinguishes between single-$\mathbf{Q}$ and double-$\mathbf{Q}$ order. Specifically, a Hubbard-Stratonovich transformation of this term reveals the nematic order parameter $\langle\phi_{\mu\nu}\rangle \propto \langle \mathbf{M}^X_\mu \mathbf{M}^X_\nu\rangle - \langle \mathbf{M}^Y_\mu \mathbf{M}^Y_\nu\rangle$, a rank-2 tensor in orbital space that breaks the tetragonal symmetry of the system by making $X \neq Y$. The term with coefficient $u^{\rho\nu\eta\mu}$ is related to Gaussian magnetic fluctuations in both SDW channels, while the term with coefficient $w^{\rho\nu\eta\mu}$ mainly distinguishes between the two types of double-$\mathbf{Q}$ order [36]. Eq. (4) is the multi-orbital generalization of the magnetic free energy previously obtained in effective low-energy models in the band basis, where the coefficient g becomes a scalar [13].

It is now possible to compute the static nematic susceptibility $\chi^{\rho\nu\eta\mu}_{\rm nem} \propto \langle\phi_{\rho\nu}\phi_{\eta\mu}\rangle$ in the paramagnetic phase

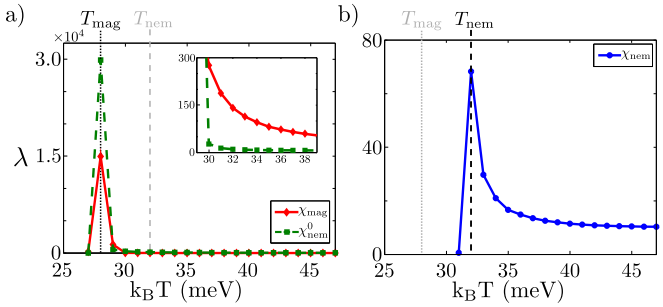

FIG. 2. (Color online) The largest eigenvalues λ of **(a)** the bare nematic susceptibility $\chi^{\rho\nu\eta\mu}_{\rm nem,0}$, the $\mathbf{Q}_{X/Y}$ magnetic propagator $\chi_{\rm mag}$, and **(b)** the full nematic susceptibility $\chi^{\rho\nu\eta\mu}_{\rm nem}$ as a function of T for the case $n = 6$. The inset in **(a)** shows the upturn of the magnetic susceptibility as it diverges.

(see Appendix B for details of the derivation):

$$\chi^{\rho\nu\eta\mu}_{\rm nem} = \chi^{\eta\alpha\mu\beta}_{\rm nem,0}\left(\delta_{\rho\beta}\delta_{\nu\alpha} - g^{\rho\nu\gamma\delta}\chi^{\gamma\alpha\delta\beta}_{\rm nem,0}\right)^{-1}, \quad (5)$$

$$\chi^{\rho\nu\eta\mu}_{\rm nem,0} \equiv \frac{1}{2}\sum_{q,i=X,Y}\chi^{\rho\nu}_i(q)\chi^{\eta\mu}_i(-q)\,. \quad (6)$$

The orbitally-resolved nematic susceptibility $\chi^{\rho\nu\eta\mu}_{\rm nem}$ is a rank-4 tensor that generalizes the scalar nematic susceptibility derived previously for effective low-energy models [38–40, 43]. The impact of the magnetic fluctuations encoded in the coefficient $g^{\rho\nu\gamma\delta}$ is clear: if this term were absent, then the (bare) nematic susceptibility would be merely a higher-order convolution of the magnetic propagator, $\chi^{\rho\nu\eta\mu}_{\rm nem,0}$, and therefore diverge at the same T as the SDW susceptibility. To establish whether the nematic susceptibility diverges already in the paramagnetic phase, one needs to compute its leading eigenvalue $\lambda^{(n)}$ from $\chi^{\rho\nu\eta\mu}_{\rm nem}\Phi^{(n)}_{\rho\nu} = \lambda^{(n)}\Phi^{(n)}_{\eta\mu}$, with $n = 1, ..., N^2_{\rm orb}$. The structure of the corresponding eigen-matrix $\Phi^{(n)}_{\eta\mu}$ reveals which orbitals promote the nematic instability, and which orbitals favor a double-$\mathbf{Q}$ structure with no underlying nematicity. We note that in principle the Gaussian fluctuations associated with the term with coefficient $u^{\rho\nu\eta\mu}$ can also renormalize the magnetic propagator $\chi^{\rho\nu}_i$. However, because this effect merely renormalizes the SDW transition temperature, we do not include it hereafter.

Equation (5) is the RPA-generalized nematic susceptibility, which can be compared on equal-footing with other RPA instabilities of a weakly-interacting system described by a multi-orbital Hubbard model. We apply this formalism to a five-orbital model for the iron-based superconductors and contrast the nematic susceptibility to the ferro-orbital RPA susceptibility. The hopping parameters are those from Ref. [44], whereas the interactions are set to $U = 0.95$ eV and $J = U/4$ [34]. Small changes in these parameters do not alter our main results. The Fermi surface for the occupation number $n = 6$ is presented in Fig. 1, consisting of three hole pockets at the center and the corner of the Brillouin zone, and two electron pockets at the borders of the Brillouin zone. that the d_{xy} hole pocket at (π, π) is not present in all materials, as it depends on the Fe-As distance [41, 42].

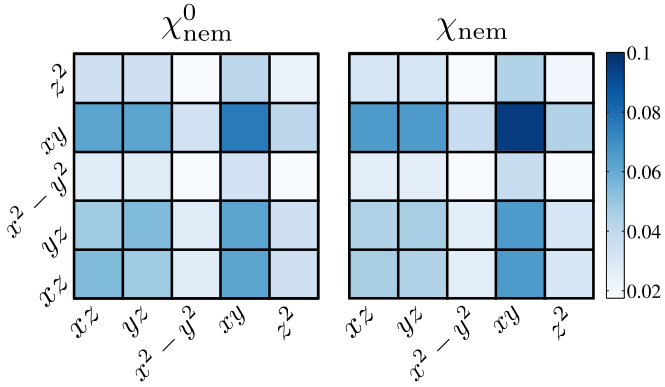

FIG. 3. (Color online) Color plot of the normalized elements of the eigen-matrix $\Phi^{(n)}_{\eta\mu}$ corresponding to the leading eigenvalue of the bare (left) and of the full (right) nematic susceptibilities. The dominant contributions arise from the d_{xz}, d_{yz}, and d_{xy} orbital, with the d_{xy} being the most important for nematicity.

We evaluate Eqs. (3) and (5) numerically as functions of T for various values of the occupation number n. Consider first $n = 6$: in Fig. 2(a), we plot the T dependence of the largest eigenvalue of the static magnetic propagator $\chi^{\mu\nu}_i(0)$ as well as the largest eigenvalue of the *bare* nematic susceptibility $\chi^{\rho\nu\eta\mu}_{\rm nem,0}$. Despite having different T dependencies, both eigenvalues diverge at the same temperature $T_{\rm mag}$, confirming our assertion that the standard RPA is blind to the nematic instability. In Fig. 2(b), we plot the largest eigenvalue of the *full* nematic susceptibility $\chi^{\rho\nu\eta\mu}_{\rm nem}$, as given by Eq. (5). Clearly, the eigenvalue diverges at $T > T_{\rm mag}$: this is exactly the nematic transition temperature $T_{\rm nem}$.

Interestingly, our results reveal a relatively small splitting between $T_{\rm nem}$ and $T_{\rm mag}$, with $T_{\rm nem} \approx 1.14T_{\rm mag}$, which resembles the small T-range in which a nematic-paramagnetic phase is observed experimentally in the iron pnictides [26]. We caution, however, that this value should be understood as an upper boundary for the splitting between the nematic and the actual magnetic transition, since $\widetilde{T}_{\rm mag}$ calculated inside the nematic state is generally larger than $T_{\rm mag}$ calculated in the tetragonal state. Furthermore, the value for $T_{\rm mag}$ obtained via RPA overestimates the actual transition temperature due to the absence of Gaussian fluctuations, as discussed above.

While the largest eigenvalue $\lambda^{(n)}$ determines $T_{\rm nem}$, the structure of the corresponding 5×5 eigen-matrix $\Phi^{(n)}_{\eta\mu}$ reveals the orbital-resolved nematic order parameter driving the transition, since $\Phi^{(n)}_{\eta\mu} \propto \langle \mathbf{M}^X_\eta \mathbf{M}^X_\mu \rangle - \langle \mathbf{M}^Y_\eta \mathbf{M}^Y_\mu \rangle$. In Fig. 3 we plot the normalized elements of the leading eigen-matrix $\Phi^{(n)}_{\eta\mu}$ for both the full and the bare nematic susceptibility – which, as shown above, contains information only about the magnetic instability. In both cases, the dominant processes involve the d_{xz}, d_{yz}, and d_{xy} orbitals.

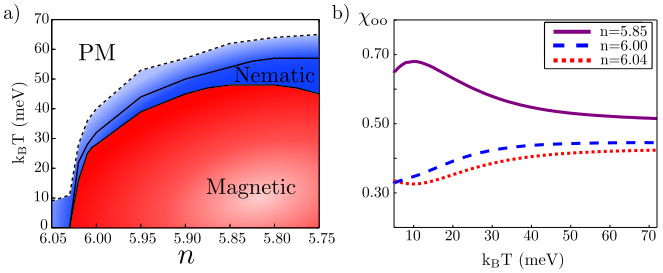

FIG. 4. (Color online) **(a)** Occupation number-temperature (n, T) phase diagram for the bare magnetic and nematic phase transitions, evidencing the narrow region displaying nematic-paramagnetic order. The solid $T_{\rm nem}$ line takes into account only the contribution from low-energy ($\Omega_n = 0$) magnetic fluctuations, whereas the dashed line includes contributions from higher energies ($\Omega < \Omega_c = 1$ eV). For $n < 5.75$, an incommensurate magnetic order appears. **(b)** Ferro-orbital order susceptibility $\chi_{\rm oo}$ a function of T for various values of the occupation number n. In contrast to the nematic susceptibility shown in Fig. 2, $\chi_{\rm oo}$ is nearly featureless and T-independent at low energies.

There is however one important difference: the relative weight of the d_{xy} orbital is larger for $\chi^{\rho\nu\eta\mu}_{\rm nem}$ than for $\chi^{\rho\nu\eta\mu}_{\rm nem,0}$, i.e. while the three orbitals seem to contribute equally to drive the magnetic instability, the d_{xy} orbital plays a more important role in driving the nematic instability. We interpret this in terms of the nesting properties of the orbital content of the Fermi surface in Fig. 1: while the d_{xy} hole-pocket at (π, π) can form a single-$\mathbf{Q}$ SDW by combining with either the X or Y electron-pockets, since both have d_{xy} spectral weight, the two d_{xz}/d_{yz} hole-pockets at $(0, 0)$ can form a double-$\mathbf{Q}$ SDW by combining with both the X and Y pockets, since they have d_{yz} and d_{xz} spectral weight, respectively.

Having analyzed the $n = 6$ case, we present in Fig. 4(a) the complete (n, T) phase diagram for the magnetic and nematic transitions. We restrict our analysis to $n > 5.75$, since below this value we find incommensurate magnetic order. Accounting for the nematic transition in this regime requires changes in the formalism beyond the scope of this work. Note that, in contrast to experiments, $T_{\rm mag}$ is not peaked at $n = 6$. This is likely due to the absence of disorder effects introduced by doping, which are known to suppress $T_{\rm mag}$ [45, 46]. Most importantly, across the entire phase diagram the nematic transition line tracks closely the magnetic transition line, in agreement with the phase diagrams of the iron pnictides.

An important issue in obtaining this phase diagram is that, as shown in Eq. (6), the computation of the nematic susceptibility requires summing the magnetic fluctuations not only over the entire Brillouin zone, but also over energy (i.e. over Matsubara frequencies). Although the propagator $\chi^{\mu\nu}_i(\mathbf{q}, \Omega_n)$ is strongly peaked at $\Omega_n = 0$ (see Appendix C), within RPA it saturates to a finite value for large energies [see Eq. (3)], requiring a frequency cutoff Ω_c. Near a finite-T magnetic transition, due to the very sharp peak in $\chi^{\mu\nu}_i(\mathbf{Q}_{X/Y}, \Omega_n)$, it is reasonable to take only the $\Omega_n = 0$ contribution – the low-energy magnetic fluctuations – resulting in the solid line of Fig. 4. However, near the region where $T_{\rm mag} \to 0$, ignoring the high-energy magnetic fluctuations ($\Omega_n \neq 0$) is not justified. To address this problem, we introduce a cutoff $\Omega_c = 1$ eV, at which the propagator reaches values close to its saturation value, as shown in Appendix C. The corresponding nematic transition line is shown as a dashed line in Fig. 4. Near the regime where the magnetic transition takes place at finite T, the only effect of the cutoff is to increase the nematic transition temperature, as expected. However, near the regime where $T_{\rm mag} \to 0$, the nematic transition is stabilized even in the absence of long-range magnetic order. Although the precise value of $T_{\rm nem}$ depends on the cutoff value, the main result is that higher-energy magnetic fluctuations are essential to promote nematic order without magnetic order. In this regard, it is interesting to note that, in FeSe, the only parent material in which nematic order is observed in the absence of magnetic order, NMR measurements find no evidence for low-energy magnetic fluctuations [47, 48], whereas neutron scattering reports sizable fluctuations at modest energy values [49, 50].

A remaining question is whether or not the spin-driven nematic instability is the leading instability of the system. In particular, an ongoing debate [2, 37, 51–54] concerning iron-based materials is whether ferro-orbital order, signaled by an unequal occupation of the d_{xz} and d_{yz} orbitals, $\Delta n \equiv n_{xz} - n_{yz} \neq 0$, could drive the nematic transition, instead of the spin-driven mechanism explored above. To investigate this issue, we calculate the $\mathbf{q} = 0$ static component of the RPA orbital order susceptibility, $\chi_{\rm oo}(\mathbf{q}) = \langle \Delta n(\mathbf{q}) \Delta n(-\mathbf{q}) \rangle$ for the multi-orbital Hubbard model [31], of which a brief derivation is included in Appendix D. As shown in Fig. 4(b), our results reveal a nearly T-independent $\chi_{\rm oo}$ for the doping range and interactions investigated. This is not unexpected, since for reasonable values of U and J, there is no attraction in the RPA charge channel. Therefore, within RPA, ferro-orbital order is unable to drive the nematic instability. Of course, once the coupling to magnetic fluctuations is included, which requires going beyond RPA, $\chi_{\rm oo}$ will diverge at the same T as $\chi_{\rm nem}$ [21, 31, 55]. In this regard, by effectively decoupling these two channels, RPA provides an interesting route to investigate which instability is the leading one – at least for weak or moderate interactions.

In summary, we developed an appropriate extension of the RPA approach to obtain the orbital-resolved spin-driven nematic susceptibility of an arbitrary multi-orbital Hubbard model. Application to the case of iron-based superconductors reveals that the leading instability of the system is an interaction-driven nematic phase. The d_{xy} orbital plays a leading role in promoting the nematic instability, and higher-energy magnetic fluctuations are essential to stabilize nematic order in the absence of long-range magnetic order. Comparison with

other RPA susceptibilities reveals that the nematic and magnetic transitions follow each other closely, and that the ferro-orbital susceptibility does not diverge on its own. More generally, our formalism can also be combined with first-principle approaches to search for other materials that may display electronic nematicity. Furthermore, because interactions appear only in the determination of the magnetic propagator, Eq. (3), this formalism can be combined with other approaches that specifically include moderate electronic interactions, such as DFT+U or LDA+DMFT [32, 33].

ACKNOWLEDGMENTS

The authors are grateful to A. V. Chubukov, L. Fanfarillo, M. Schütt, P. Orth, and B. Valenzuela for discussions. MHC and BMA acknowledge financial support from a Lunbeckfond fellowship (grant A9318). RMF and JK are supported by the U.S. Department of Energy, Office of Science, Basic Energy Sciences, under award number DE-SC0012336.

Appendix A: Fourth order coefficients

To derive the form of the free energy given in Eqs. (2) and (4) in the main text, we perform a Hubbard-Stratonovich (HS) decoupling thereby obtaining the electron-mediated interactions between the magnetic order parameters. Formally the HS decoupling relies on inserting unity in the partition function, where unity, in the present case, is given by

$$\begin{aligned}\mathbb{1} = \int \mathcal{D}[\mathbf{M}^X_{\mu\nu}, \mathbf{M}^Y_{\mu\nu}] \\ \exp\Big[- \int_q \big(\mathbf{M}^X_{\mu\nu}(q) \left(U^{-1}\right)^{\mu\nu}_{\rho\lambda} \mathbf{M}^X_{\rho\lambda}(-q) \\ + \mathbf{M}^Y_{\mu\nu}(q) \left(U^{-1}\right)^{\mu\nu}_{\rho\lambda} \mathbf{M}^Y_{\rho\lambda}(-q) \big) \Big] , \end{aligned} \tag{A1}$$

and $\int \mathcal{D}[\mathbf{M}^X_{\mu\nu}, \mathbf{M}^Y_{\mu\nu}]$ is chosen such that the path-integral evaluates to unity and $q = (\mathbf{q}, \Omega_n)$ (Ω_n being a bosonic Matsubara frequency). The electrons are then integrated out resulting in an effective action for the magnetic order

$$\begin{aligned}\mathcal{S}_{\text{eff}}[\mathbf{M}^X_{\mu\nu}, \mathbf{M}^Y_{\mu\nu}] = \sum_i \int_q \mathbf{M}^i_{\mu\nu}(q) \left(U^{-1}\right)^{\mu\nu}_{\rho\lambda} \mathbf{M}^i_{\rho\lambda}(-q) \\ - \operatorname{Tr} \ln \left[\mathbb{G}^0_{\mu\nu}(k)^{-1} - \mathcal{V}_{\mu\nu}(q) \right] , \end{aligned} \tag{A2}$$

where $i = X, Y$, μ and ν are orbital indices, $k = (\mathbf{k}, \omega_n)$, $\omega_n = (2n+1)\pi T$ is the fermionic Matsubara frequency, and the trace is over all external indices (the spin indices have been suppressed, the Green's function is diagonal in spin). $\mathbb{G}^0_{\mu\nu}(k)$ is the matrix Green's function, obtained from the first term in Eq. (1) of the main text, and $\mathcal{V}$ originates from the coupling between the magnetic order parameters and the electrons, the second term. In the basis

$$\Psi(\mathbf{k}) = \begin{pmatrix} \psi(\mathbf{k}) \\ \psi(\mathbf{k}+\mathbf{Q}_X) \\ \psi(\mathbf{k}+\mathbf{Q}_Y) \\ \psi(\mathbf{k}+\mathbf{Q}_X+\mathbf{Q}_Y) \end{pmatrix} \tag{A3}$$

these are given by the matrices

$$\mathbb{G}^0_{\mu\nu}(k) = \begin{pmatrix} \mathcal{G}^0_{\mu\nu}(k+q) & 0 & 0 & 0 \\ 0 & \mathcal{G}^0_{\mu\nu}(k+q+\mathbf{Q}_X) & 0 & 0 \\ 0 & 0 & \mathcal{G}^0_{\mu\nu}(k+q+\mathbf{Q}_Y) & 0 \\ 0 & 0 & 0 & \mathcal{G}^0_{\mu\nu}(k+q+\mathbf{Q}_X+\mathbf{Q}_Y) \end{pmatrix} \tag{A4}$$

$$\mathcal{V}_{\mu\nu}(q) = \begin{pmatrix} 0 & -\frac{1}{2}\mathbf{M}^X_{\mu\nu}(q)\cdot\boldsymbol{\sigma}_{\alpha\beta} & -\frac{1}{2}\mathbf{M}^Y_{\mu\nu}(q)\cdot\boldsymbol{\sigma}_{\alpha\beta} & 0 \\ -\frac{1}{2}\mathbf{M}^X_{\mu\nu}(q)\cdot\boldsymbol{\sigma}_{\alpha\beta} & 0 & 0 & -\frac{1}{2}\mathbf{M}^Y_{\mu\nu}(q)\cdot\boldsymbol{\sigma}_{\alpha\beta} \\ -\frac{1}{2}\mathbf{M}^Y_{\mu\nu}(q)\cdot\boldsymbol{\sigma}_{\alpha\beta} & 0 & 0 & -\frac{1}{2}\mathbf{M}^X_{\mu\nu}(q)\cdot\boldsymbol{\sigma}_{\alpha\beta} \\ 0 & -\frac{1}{2}\mathbf{M}^Y_{\mu\nu}(q)\cdot\boldsymbol{\sigma}_{\alpha\beta} & -\frac{1}{2}\mathbf{M}^X_{\mu\nu}(q)\cdot\boldsymbol{\sigma}_{\alpha\beta} & 0 \end{pmatrix} , \tag{A5}$$

where each element of the matrices should be understood as an $N_{\text{orb}} \times N_{\text{orb}}$ matrix in orbital space, with the Green function being

$$\mathcal{G}^0_{\mu\nu}(k) = \sum_m \frac{\langle \mu | m \rangle \langle m | \nu \rangle}{i\omega_n - \xi^m(\mathbf{k})} , \tag{A6}$$

where m refers to band basis and μ, ν refer to orbital basis. Expanding the trace-log to fourth order in the magnetic order parameters and applying the Pauli matrix identity

$$\sigma^i_{\alpha\beta}\sigma^j_{\beta\delta}\sigma^k_{\delta\gamma}\sigma^l_{\gamma\alpha} = 2\left(\delta^{ij}\delta^{kl} - \delta^{ik}\delta^{jl} + \delta^{il}\delta^{jk}\right) \tag{A7}$$

yields the magnetic free energy as written in Eqs. (2) and (4) of the main text, with the fourth order coefficients

$$u^{\rho\nu\eta\mu} = \frac{1}{16}\sum_k \Big(2\mathcal{G}^{\mu\rho}\mathcal{G}^{\rho\nu}_X\mathcal{G}^{\nu\eta}\mathcal{G}^{\eta\mu}_X - \mathcal{G}^{\mu\rho}\mathcal{G}^{\rho\eta}_X\mathcal{G}^{\eta\nu}_X\mathcal{G}^{\nu\mu}_X + \mathcal{G}^{\mu\rho}\mathcal{G}^{\rho\nu}_X\mathcal{G}^{\nu\eta}\mathcal{G}^{\eta\mu}_Y$$
$$+ \mathcal{G}^{\nu\rho}\mathcal{G}^{\rho\mu}_X\mathcal{G}^{\mu\eta}_{X+Y}\mathcal{G}^{\eta\nu}_X - \mathcal{G}^{\mu\rho}\mathcal{G}^{\rho\eta}_X\mathcal{G}^{\eta\nu}_{X+Y}\mathcal{G}^{\nu\mu}_Y\Big) + (X\leftrightarrow Y)\,, \tag{A8}$$

$$g^{\rho\nu\eta\mu} = -\frac{1}{16}\sum_k \Big(2\mathcal{G}^{\mu\rho}\mathcal{G}^{\rho\nu}_X\mathcal{G}^{\nu\eta}\mathcal{G}^{\eta\mu}_X - \mathcal{G}^{\mu\rho}\mathcal{G}^{\rho\eta}_X\mathcal{G}^{\eta\nu}_X\mathcal{G}^{\nu\mu}_X - \mathcal{G}^{\mu\rho}\mathcal{G}^{\rho\nu}_X\mathcal{G}^{\nu\eta}\mathcal{G}^{\eta\mu}_Y$$
$$- \mathcal{G}^{\nu\rho}\mathcal{G}^{\rho\mu}_X\mathcal{G}^{\mu\eta}_{X+Y}\mathcal{G}^{\eta\nu}_X + \mathcal{G}^{\mu\rho}\mathcal{G}^{\rho\eta}_X\mathcal{G}^{\eta\nu}_{X+Y}\mathcal{G}^{\nu\mu}_Y\Big) + (X\leftrightarrow Y)\,, \tag{A9}$$

$$w^{\rho\nu\eta\mu} = \frac{1}{16}\sum_k \Big(-2\mathcal{G}^{\mu\rho}\mathcal{G}^{\rho\eta}_X\mathcal{G}^{\eta\nu}\mathcal{G}^{\nu\mu}_Y + 2\mathcal{G}^{\nu\rho}\mathcal{G}^{\rho\eta}_X\mathcal{G}^{\eta\mu}\mathcal{G}^{\mu\nu}_Y - 2\mathcal{G}^{\eta\rho}\mathcal{G}^{\rho\mu}_X\mathcal{G}^{\mu\nu}_{X+Y}\mathcal{G}^{\nu\eta}_X + 2\mathcal{G}^{\eta\rho}\mathcal{G}^{\rho\nu}_X\mathcal{G}^{\nu\mu}_{X+Y}\mathcal{G}^{\mu\eta}_X$$
$$+ \mathcal{G}^{\rho\mu}\mathcal{G}^{\mu\eta}_Y\mathcal{G}^{\eta\nu}_{X+Y}\mathcal{G}^{\nu\rho}_X + \mathcal{G}^{\rho\nu}\mathcal{G}^{\nu\eta}_Y\mathcal{G}^{\eta\mu}_{X+Y}\mathcal{G}^{\mu\rho}_X + \mathcal{G}^{\mu\rho}\mathcal{G}^{\rho\nu}_X\mathcal{G}^{\nu\eta}_{X+Y}\mathcal{G}^{\eta\mu}_Y + \mathcal{G}^{\nu\rho}\mathcal{G}^{\rho\mu}_X\mathcal{G}^{\mu\eta}_{X+Y}\mathcal{G}^{\eta\nu}_Y\Big)\,, \tag{A10}$$

where repeated orbital indices are not summed. Here all the Green functions are implicit functions of k and $\mathcal{G}^{\mu\nu}_j(k) = \mathcal{G}^{\mu\nu}(k+\mathbf{Q}_j)$ and $\sum_k = T/N_{\mathbf{k}}\sum_{\mathbf{k}}\sum_{\omega_n}$.

Appendix B: Nematic susceptibility

Preparing for an additional HS-decoupling we introduce two bosonic fields $\psi_{\rho\nu}$ and $\phi_{\rho\nu}$ with the partition function

$$\mathcal{Z} = \int \mathcal{D}\phi\mathcal{D}\psi \exp\Big[\frac{1}{2}\left(u^{\rho\nu\eta\mu}\right)^{-1}\psi_{\rho\nu}\psi_{\eta\mu} - \frac{1}{2}\left(g^{\rho\nu\eta\mu}\right)^{-1}\phi_{\rho\nu}\phi_{\eta\mu}\Big], \tag{B1}$$

with integration measures chosen appropriately such that $\mathcal{Z}=1$. By performing the shifts

$$\psi_{\rho\nu} \to \psi_{\rho\nu} - u^{\rho\nu\eta\mu}\left(\mathbf{M}^X_\eta\cdot\mathbf{M}^X_\mu + \mathbf{M}^Y_\eta\cdot\mathbf{M}^Y_\mu\right), \tag{B2}$$
$$\phi_{\rho\nu} \to \psi_{\rho\nu} + g^{\rho\nu\eta\mu}\left(\mathbf{M}^X_\eta\cdot\mathbf{M}^X_\mu - \mathbf{M}^Y_\eta\cdot\mathbf{M}^Y_\mu\right), \tag{B3}$$

the terms quartic in $\mathbf{M}$ cancel accordingly. Following the standard procedure we introduce a field $(h_{\rho\nu})$ conjugate to $\mathbf{M}^X_\rho\cdot\mathbf{M}^X_\nu - \mathbf{M}^Y_\rho\cdot\mathbf{M}^Y_\nu$ and define $\widetilde{\phi}_{\rho\nu} = \phi_{\rho\nu} + h_{\rho\nu}$. The resulting action is then

$$\mathcal{S}[\mathbf{M}^i_\mu,\psi_{\mu\nu},\phi_{\mu\nu}] = \sum_{q,i=X,Y}\left(r^{\mu\nu}_i(q)+\psi_{\mu\nu}\right)\mathbf{M}^i_\mu\cdot\mathbf{M}^i_\nu - \frac{1}{2}\left(u^{\rho\nu\eta\mu}\right)^{-1}\psi_{\rho\nu}\psi_{\eta\mu} + \frac{1}{2}\left(g^{\rho\nu\eta\mu}\right)^{-1}\left(\widetilde{\phi}_{\rho\nu}-h_{\eta\mu}\right)\left(\widetilde{\phi}_{\eta\mu}-h_{\eta\mu}\right) - \widetilde{\phi}_{\rho\nu}\left(\mathbf{M}^X_\rho\cdot\mathbf{M}^X_\nu - \mathbf{M}^Y_\rho\cdot\mathbf{M}^Y_\nu\right). \tag{B4}$$

Here $r^{\mu\nu}_i(q) = (U^\mu_\nu)^{-1} + \sum_k \mathcal{G}^{\nu\mu}(k)\mathcal{G}^{\mu\nu}_i(k+q)$ and $\mathcal{G}^{\mu\nu}_i(k)\equiv\mathcal{G}^{\mu\nu}(k+\mathbf{Q}_i)$. It is now straightforward to compute the nematic susceptibility:

$$\chi^{\rho\nu\eta\mu}_{\rm nem} = \lim_{h\to0}\left(\frac{\delta^2\ln\mathcal{Z}}{\delta h_{\rho\nu}\delta h_{\eta\mu}}\right) = \left(g^{\rho\nu\iota\kappa}g^{\eta\mu\phi\lambda}\right)^{-1}\langle\phi_{\iota\kappa}\phi_{\phi\lambda}\rangle - \left(g^{\rho\nu\eta\mu}\right)^{-1}, \tag{B5}$$

where we used the fact that $\langle\phi_{\rho\nu}\rangle = 0$ as we are above the nematic instability. To continue we note that

$$\frac{\delta^2 F}{\delta\phi_{\rho\nu}\delta\phi_{\eta\mu}} = \langle\phi_{\rho\nu}\phi_{\eta\mu}\rangle^{-1}, \tag{B6}$$

where the free energy is

$$F = -T\ln\mathcal{Z}, \tag{B7}$$

obtained by integrating out the magnetic degrees of freedom and taking the large N limit. We find the effective action

$$\mathcal{S}_{\rm eff}[\psi_{\mu\nu},\phi_{\mu\nu}] = \frac{1}{2}\left(g^{\rho\nu\eta\mu}\right)^{-1}\phi_{\rho\nu}\phi_{\eta\mu} + \frac{1}{2}{\rm Tr}\ \ln\left[\chi^{-1}_{\iota\kappa,Y}\chi^{-1}_{\kappa\lambda,X} - \phi_{\iota\kappa}\phi_{\kappa\lambda} + \chi^{-1}_{\iota\kappa,Y}\phi_{\kappa\lambda} - \phi_{\iota\kappa}\chi^{-1}_{\kappa\lambda,X}\right], \tag{B8}$$

where we have ignored the Gaussian fluctuations $\psi_{\rho\nu}$ and $(\chi^{\mu\nu}_i(q))^{-1} = r^{\mu\nu}_i(q)$. Finally

$$\langle\phi_{\rho\nu}\phi_{\eta\mu}\rangle^{-1} = \left(g^{\rho\nu\eta\mu}\right)^{-1} - \frac{1}{2}\sum_{q,i=X,Y}\chi_{\rho\mu,i}(q)\chi_{\nu\eta,i}(-q) \tag{B9}$$

and after some manipulations we arrive at the expression given in the text for the nematic susceptibility.

Appendix C: Frequency dependence of the magnetic susceptibility

In this section we illustrate the frequency dependence of the magnetic propagator at various temperatures for representative filling factors of the (n,T) phase diagram (Fig. 4(a) of the main text). Because the magnetic propagator peaks at $(\pi,0)/(0,\pi)$, we focus on $\mathbf{Q}_X$. For $n=5.90$ as we approach the instability (at $k_{\rm B}T = 45$ meV), the frequency dependence of the propagator $\sum_{\mu\nu}\chi^{\mu\nu}_X(\mathbf{Q}_X,\Omega_n)$ has the form shown in Fig. 5, where the bosonic Matsubara frequency is given by $\Omega_n = 2\pi nT$. The gray area denotes the region included

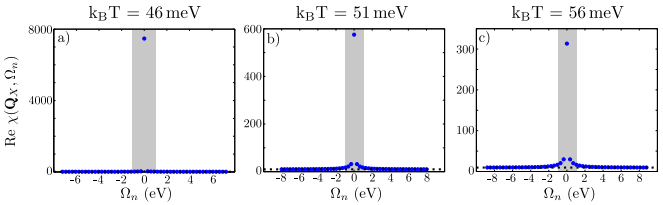

FIG. 5. Frequency dependence of the magnetic propagator $\sum_{\mu\nu}\chi_X^{\mu\nu}(\mathbf{Q}_X,\Omega_n)$ for $n = 5.90$ at different temperatures. The parameters used are quoted in the main text. The magnetic instability takes place at $k_BT = 45$ meV. From (a) we see that the contribution to the bare nematic susceptibility comes mostly from the zero frequency part of the magnetic susceptibility.

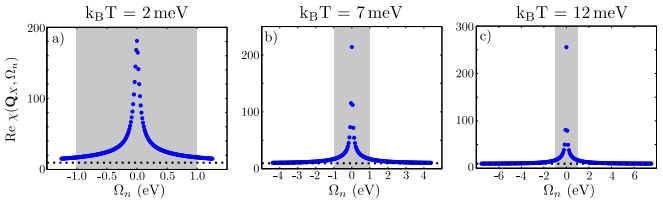

FIG. 6. Frequency dependence of the magnetic propagator $\sum_{\mu\nu}\chi_X^{\mu\nu}(\mathbf{Q}_X,\Omega_n)$ for $n = 6.04$ at different temperatures. The parameters used are quoted in the main text. As is evident in (a), the peak broadens as zero temperature is approached. However, even at higher temperatures, shown in (b) and (c), finite Matsubara frequencies provide considerable contributions to the bare nematic susceptibility.

in the cut-off $\Omega_c = 1\,\text{eV}$, and the dotted line indicates $\sum_{\mu\nu}\chi_X^{\mu\nu}(\mathbf{Q}_X,\Omega_n\to\infty)$. The plots in Fig. 5 justify the statement made in the main text that near a finite-temperature magnetic transition, one can safely neglect the higher frequency contributions.

To illustrate the importance of including high frequency contributions in the case where magnetic order is absent, in Fig. 6 we also plot the frequency dependence of the magnetic propagator for $n = 6.04$. It is clear that the peak is broadened, implying that it is no longer justified to ignore the contributions originating from finite frequencies.

Appendix D: Derivation of the ferro-orbital order susceptibility

Ferro-orbital order is characterized by the breaking of the degeneracy between the d_{xz} and d_{yz} orbitals. In the itinerant framework this is seen by an inequivalent occupation of the two orbitals, i.e. $n_{xz} \neq n_{yz}$. Defining $\Delta n(q) \equiv n_{xz}(q) - n_{yz}(q)$ as in the main text, the ferro-orbital susceptibility is given by $\langle \Delta n(q)\Delta n(-q)\rangle$. Using the definition of $\Delta n(q)$, we find that this is nothing but a linear combination of specific components of the charge susceptibility, $(\chi^{\text{c}})^{\mu\nu}_{\rho\lambda}$. In the standard RPA approach, the full expression is [31, 55]

$$\begin{aligned}\chi_{\text{oo}} = &(\chi^{\text{c}}_{\text{RPA}})^{xz,xz}_{xz,xz} + (\chi^{\text{c}}_{\text{RPA}})^{yz,yz}_{yz,yz} \\ &- (\chi^{\text{c}}_{\text{RPA}})^{xz,yz}_{xz,yz} - (\chi^{\text{c}}_{\text{RPA}})^{yz,xz}_{yz,xz}\,, \end{aligned} \tag{D1}$$

where the RPA charge susceptibility is given by the usual expression [25]

$$(\chi^{\text{c}}_{\text{RPA}})^{\mu\nu}_{\rho\lambda} = \Big([1+\chi_0 U_c]^{-1}\Big)^{\mu\delta}_{\rho\gamma}(\chi_0)^{\delta\nu}_{\gamma\lambda}\,, \tag{D2}$$

where χ_0 is the standard particle-hole bubble

$$(\chi_0(q))^{\mu\nu}_{\rho\lambda} = -\sum_k \mathcal{G}^{\mu\nu}(k)\mathcal{G}^{\rho\lambda}(k+q) \tag{D3}$$

and U_c is the interaction matrix in the charge channel. The latter differs from the interaction in the SDW channel and is given by ($a \neq b$)

$$(U_c)^{aa}_{aa} = U\,, \tag{D4}$$
$$(U_c)^{aa}_{bb} = 2U' - J = 2U - 5J\,, \tag{D5}$$
$$(U_c)^{ab}_{ab} = 2J - U' = 4J - U\,, \tag{D6}$$
$$(U_c)^{ba}_{ab} = J' = J\,. \tag{D7}$$

We note that, due to the implicit summation over repeated indices in Eq. (D2), all orbitals contribute to the RPA orbital order susceptibility. The static part of Eq. (D1) at $\mathbf{q} = 0$ is the quantity plotted in Fig. 4(b) in the main text.

[1] P. Chandra, P. Coleman, and A. I. Larkin, Phys. Rev. Lett. **64**, 88 (1990).
[2] R. M. Fernandes, A. V. Chubukov, and J. Schmalian, Nat. Phys. **10**, 97 (2014).
[3] S. A. Kivelson, I. P. Bindloss, E. Fradkin, V. Oganesyan, J. M. Tranquada, A. Kapitulnik, and C. Howald, Rev. Mod. Phys. **75**, 1201 (2003).
[4] J. Chu, J. G. Analytis, K. De Greve, P. L. McMahon, Z. Islam, Y. Yamamoto, and I. R. Fisher, Science **329**, 824 (2010).
[5] T.-M. Chuang, M. P. Allan, J. Lee, Y. Xie, N. Ni, S. L. Bud'ko, G. S. Boebinger, P. C. Canfield, and J. C. Davis, Science **327**, 181 (2010).
[6] J. Chu, H. Kuo, J. G. Analytis, and I. R. Fisher, Science **337**, 710 (2012).
[7] C. Mirri, A. Dusza, S. Bastelberger, M. Chinotti, L. Degiorgi, J. H. Chu, H. H. Kuo, and I. R. Fisher, Phys. Rev. Lett. **115**, 107001 (2015).
[8] M. Yi, D. Lu, J.-H. Chu, J. G. Analytis, A. P. Sorini, A. F. Kemper, B. Moritz, S.-K. Mo, R. G. Moore, M. Hashimoto, W. S. Lee, Z. Hussain, T. P. Devereaux, I. R. Fisher, Z.-X. Shen, Proc. Nat. Acad. Sci. 2011 **108**, 6878 (2011).

[9] S. Kasahara, H. J. Shi, K. Hashimoto, S. Tonegawa, Y. Mizukami, T. Shibauchi, K. Sugimoto, T. Fukuda, T. Terashima, A. H. Nevidomskyy, and Y. Matsuda, Nature **486**, 382 (2012).

[10] R. Daou, J. Chang, D. LeBoeuf, O. Cyr-Choinière, F. Laliberté, N. Doiron-Leyraud, B. J. Ramshaw, R. Liang, D. A. Bonn, W. N. Hardy, and L. Taillefer, Nature, **463**, 519 (2010).

[11] V. Hinkov, D. Haug, B. Fauque, P. Bourges, Y. Sidis, A. Ivanov, C. Bernhard, C. T. Lin, and B. Keimer, Science **319**, 597 (2008).

[12] M. J. Lawler, K. Fujita, L. Jhinhwan, A. R. Schmidt, Y. Kohsaka, K. C. Koo, H. Eisaki, S. Uchida, J. C. Davis, J. P. Sethna, and K. Eun-Ah, Nature **466**, 347 (2010).

[13] R. M. Fernandes, A. V. Chubukov, J. Knolle, I. Eremin, and J. Schmalian, Phys. Rev. B **85**, 024534 (2012).

[14] C. Fang, H. Yao, W.-F. Tsai, J. P. Hu, and S. A. Kivelson, Phys. Rev. B **77**, 224509 (2008).

[15] C. Xu, M. Müller, and S. Sachdev, Phys. Rev. B **78**, 020501(R) (2008).

[16] E. Abrahams and Q. Si, J. Phys.: Condens. Matter **23**, 223201 (2011).

[17] S. A. Kivelson, E. Fradkin, and V. J. Emery, Nature **393**, 550 (1998).

[18] L. Nie, G. Tarjus, and S. A. Kivelson, PNAS **111**, 7980 (2014).

[19] Y. Wang and A. Chubukov, Phys. Rev. B **90**, 035149 (2014).

[20] I. Eremin and A. V. Chubukov, Phys. Rev. B **81**, 024511 (2011)

[21] L. Fanfarillo, A. Cortijo, and B. Valenzuela, Phys. Rev. B **91**, 214515 (2015).

[22] S. Okamoto, D. Sénéchal, M. Chivelli, and A.-M. S. Tremblay, Phys. Rev. B **82**, 180511(R) (2010).

[23] S.-Q. Su, and T. A. Maier, Phys. Rev. B **84**, 220506(R) (2011).

[24] K. Kuroki, S. Onari, R. Arita, H. Usui, Y. Tanaka, H. Kontani, and H. Aoki, Phys. Rev. Lett. **101**, 087004 (2008).

[25] A. F. Kemper, T. A. Maier, S. Graser, H-P. Cheng, P. J. Hirschfeld, and D. J. Scalapino, New J. Phys. **12** 073030 (2010).

[26] K. Ishida, Y. Nakai and H. Hosono, J. Phys. Soc. Japan **78**, 062001 (2009); D. C. Johnston, Adv. Phys. **59**, 803 (2010); J. Paglione and R. L. Greene, Nature Phys. **6**, 645 (2010); P. C. Canfield and S. L. Bud'ko, Annu. Rev. Cond. Mat. Phys. **1**, 27 (2010); H. H. Wen and S. Li, Annu. Rev. Cond. Mat. Phys. **2**, 121 (2011).

[27] A. V. Chubukov, R. M. Fernandes, and J. Schmalian, Phys. Rev. B **91**, 201105(R) (2015).

[28] J. K. Glasbrenner, I. I. Mazin, H. O. Jeschke, P. J. Hirschfeld, R. M. Fernandes, and R. Valenti, Nature Phys. *in press*, doi:10.1038/nphys3434.

[29] F. Wang, S. Kivelson, and D.-H. Lee, Nature Phys. *in press*, doi:10.1038/nphys3456.

[30] R. Yu and Q. Si, Phys. Rev. Lett. **115**, 116401 (2015).

[31] Y. Yamakawa, S. Onari, and H. Kontani, arXiv:1509.01161.

[32] H. Park, K. Haule, and G. Kotliar, Phys. Rev. Lett. **107**, 137007 (2011)

[33] A. Georges, L. de' Medici, and J. Mravlje, Annu. Rev. Cond. Mat. Phys. **4**, 137 (2013).

[34] M. N. Gastiasoro and B. M. Andersen, Phys. Rev. B **92**, 150506(R) (2015).

[35] S. Liang, A. Moreo, and E. Dagotto, Phys. Rev. Lett. **111**, 047004 (2013).

[36] X. Wang, J. Kang, and R. M. Fernandes, Phys. Rev. B **91**, 024401 (2015).

[37] S. Onari and H. Kontani, Phys. Rev. Lett. **109**, 137001 (2012).

[38] R. M. Fernandes, L. H. VanBebber, S. Bhattacharya, P. Chandra, V. Keppens, D. Mandrus, M. A. McGuire, B. C. Sales, A. S. Sefat, and J. Schmalian, Phys. Rev. Lett. **105**, 157003 (2010).

[39] M. Khodas and A. Levchenko, Phys. Rev. B **91**, 235119 (2015).

[40] Y. Gallais and I. Paul, arXiv:1508.01319.

[41] V. Vildosola, L. Pourovskii, R. Arita, S. Biermann, and A. Georges, Phys. Rev. B **78**, 064518 (2008).

[42] M. J. Calderón, B. Valenzuela, and E. Bascones, Phys. Rev. B **80**, 094531 (2009).

[43] H. Yamase and R. Zeyher, New J. Phys. **17**, 073030 (2015).

[44] H. Ikeda, R. Arita, and J. Kuneš, Phys. Rev. B **81**, 054502 (2010).

[45] S. Liang, C. B. Bishop, A. Moreo, and E. Dagotto, arXiv:1506.00309.

[46] R. M. Fernandes, M. G. Vavilov, and A. V. Chubukov, Phys. Rev. B **85**, 140512(R) (2012).

[47] A. E. Böhmer, T. Arai, F. Hardy, T. Hattori, T. Iye, T. Wolf, H. v. Löhneysen, K. Ishida, and C. Meingast Phys. Rev. Lett. **114**, 027001 (2015).

[48] S.-H. Baek, D. V. Efremov, J. M. Ok, J. S. Kim, J. van den Brink, and B. Büchner, Nat. Mater. **14**, 210 (2014).

[49] M. C. Rahn, R. A. Ewings, S. J. Sedlmaier, S. J. Clarke, and A. T. Boothroyd, Phys. Rev. B **91**, 180501(R) (2015).

[50] Q. Wang, Y. Shen, B. Pan, Y. Hao, M. Ma, F. Zhou, P. Steffens, K. Schmalzl, T. R. Forrest, M. Abdel-Hafiez, D. A. Chareev, A. N. Vasiliev, P. Bourges, Y. Sidis, H. Cao, and J. Zhao, arXiv:1502.07544.

[51] F. Krüger, S. Kumar, J. Zaanan, and J. van den Brink, Phys. Rev. B **79**, 054504 (2009).

[52] C. C. Chen, B. Moritz, J. van den Brink, T. P. Devereaux, and R. R. P. Singh, Phys. Rev. B **80**, 180418 (2009).

[53] W. Lv, J. Wu, and P. Phillips, Phys. Rev. B **80**, 224506 (2009).

[54] C. C. Lee, W. G. Yin, and W. Ku, Phys. Rev. Lett. **103**, 267001 (2009).

[55] Z. Wang and A. H. Nevidomskyy, J. Phys.: Condens. Matter **27**, 225602 (2015).